Hindawi
Journal of Energy
Volume 2020, Article ID 7892680, 11 pages
https://doi.org/10.1155/2020/7892680

Research Article

Comparative Study of the Grid Side Converter's Control during a Voltage Dip

Hind Elaimani,[1] **Ahmed Essadki**,[1] **Noureddine Elmouhi**,[1,2] **and Rachid Chakib**[2]

[1]*Research Center of Engineering and Health Sciences and Technologies (STIS), High Normal School of Technical Education (ENSET), Mohammed V University, Rabat, Morocco*
[2]*Research Center of Higher Institute of Engineering and Business (CRI ISGA), 27 Avenue Oqba Agdal, 10090 Rabat, Morocco*

Correspondence should be addressed to Hind Elaimani; h.elaimani@gmail.com

Received 22 May 2019; Revised 31 July 2019; Accepted 9 September 2019; Published 1 February 2020

Academic Editor: Kamal Aly

The modeling and control of a wind energy conversion system based on the Doubly Fed Induction Generator DFIG is the discussed theme in this paper. The purpose of this system was to control active and reactive power converted; this control is ensured thanks to the control of the two converters. The proposed control strategies are controlled by PI regulators and the sliding mode technique. In the present work a comparison of the robustness of the 2 controls of the grid side converter (GSC) during a voltage dip is shown. The simulation is carried out using the Matlab/Simulink software with a 300 kW generator.

1. Introduction

In recent years, the wind energy has become the fastest growing renewable energy source in the world. This is mainly due to the fact that it has received thorough attention and has been considered as a way of fighting climate change. Control of the speed of the wind turbine is generally used to improve the energy production [1].

Several structures are used to control speed, structures based on asynchronous machine, synchronous machine and Doubly Fed Induction Generator known as DFIG.

The DFIG's structure is the most used, thanks to the advantages it gives. This structure is composed of a wound rotor induction generator where its stator is directly connected to the grid and its rotor is connected to the grid through two power converters [2]. Several lines of research in literature shows the classical control of the power converters; the first one rotor side converter (RSC) controls the DFIG, and the second one grid side converter (GSC) controls the DC link's voltage.

The control can be ensured using different techniques as the PI regulators, the Backstepping technique, direct power control, direct torque control and the control by sliding mode, which will be the object of this work [3, 4].

In PI, control strategy has been investigated; the synthesis of this technique is purely algebraic and uses the pole compensation based on a numerical method [1], investigating a polynomial RST controller. This method is a sophisticated one and based on pole placement technique. Sliding Mode Control (SMC) controllers have been implemented in many areas because of their excellent properties, such as insensitivity to external perturbation and parameter variation [1].

These wind generators, like most decentralized generators, are very sensitive to grid disturbances and tend to disconnect quickly. Indeed, faults in the power system, even very far from the generator, can result in short-term voltage disturbances, called voltage dips, which can lead to the disconnection of the wind system. The need to ensure the continuity of service of the WECS in the voltage dips event is all the stronger as the penetration rate in the network is high [5–7].

The aim of this paper is to compare the GSC's controls with PI and with the SM technique during a voltage dip.

Wind generators, like most decentralized generators, are very sensitive to network disturbances and tend to disconnect quickly during a voltage dip or when the frequency changes. These disconnections lead to production losses that can aggravate the situation on a network, already weakened by the incident and thus have negative consequences. It is therefore necessary to avoid this instability in the production of wind energy to ensure continuity of service [8].

The challenge is to satisfy the continuity of service during a voltage dip.

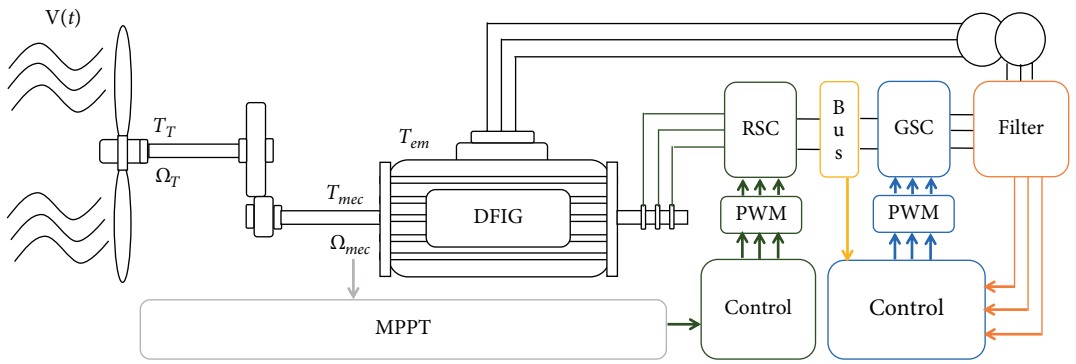

Figure 1: Schematic diagram of WECS based on DFIG.

This paper is structured as follows: first, the topology of the system studied is presented in the second section. Then, the modeling of the turbine, the doubly fed induction generator, the power converters and the filter is shown in the third, fourth and fifth sections, respectively. The sixth, seventh and eighth sections present to the controllers of the power converters using the PI regulators and the sliding mode techniques. The ninth section shows the voltage dip types. The last section is dedicated to the simulation results carried out using the Matlab/Simulink software, followed by a conclusion.

2. The Topology of the Studied System

The most suitable technology is the one based on the double-feed asynchronous machine with wound rotor, whose speed variation is done by means of the power converters located at the rotor circuit and the stator, which is connected directly to the grid (Figure 1).

3. The Turbine Modelling

3.1. Wind Model. The kinetic energy of the wind presents the source of the wind energy conversion system. The wind is equivalent to an air mass displacement field characterized by a variable speed and a random trajectory applied to the turbine. It creates forces on the surfaces of its blades; the latter generate a rotary movement of the blades.

The wind speed is given by the addition of two velocities, the first V (constant), the second $V_0(t)$ varies in turbulence as a function of time. Its expression is as follows:

$$V(t) = K + V_0(t), \tag{1}$$

$$V_0(t) = 2\sin\theta_1 + 2\sin\theta_2 + 1.5\sin\theta_3 + 0.5\sin\theta_4, \tag{2}$$

where: $\theta_1 = 2.5t - (\pi/5); \theta_2 = 4t - (\pi/3); \theta_3 = 5.4t - (\pi/12); \theta_4 = 2.5t - (\pi/12)$.

The K component represents three levels of wind velocity:

(i) $K = 6$ m/s for low wind speed;
(ii) $K = 12$ m/s for an average wind speed;
(iii) $K = 18$ m/s for high wind speed.

3.2. Aerodynamic Conversion. The wind velocity V that passes through a surface S is expressed as follows:

$$P_{aér} = \frac{1}{2}\rho S V^3, \tag{3}$$

where: ρ: air density; S: wind-swept turbine surface; its expression is as follow:

$$S = \pi R_T^2. \tag{4}$$

The turbine power P_t according to the Betz theory is given by:

$$P_T = P_{aér} C_p(\beta, \lambda). \tag{5}$$

$C_p(\beta, \lambda)$: aerodynamic efficiency of the turbine often referred to as a power factor. It is a specific coefficient to each wind turbine; it depends on the specific speed λ and the orientation angle of the blades β.

$$C_p(\lambda, \beta) = 0.5176\left(\frac{116}{\lambda_i} - 0.4\beta - 5\right)e^{-21/\lambda_i} + 0.0068\lambda, \tag{6}$$

where

$$\lambda_i = \left(\frac{1}{\lambda + 0.08\beta} - \frac{0.035}{\beta^3 + 1}\right)^{-1}$$
$$\lambda = \frac{\Omega_T R_T}{V}. \tag{7}$$

The turbine torque is defined by:

$$T_T = \frac{P_T}{\Omega_T}. \tag{8}$$

The role of the gear box is to adapt the rotation speed of the turbine to the rotation speed of the generator. Its gain is given by:

$$G = \frac{T_T}{T_{mec}} = \frac{\Omega_{mec}}{\Omega_T}. \tag{9}$$

Applying the fundamental relation of the dynamics, the generator tree is modeled by the following equation:

$$J\frac{d\Omega_{mec}}{dt} = \sum T = T_{mec} - T_{em} - T_{vis}. \tag{10}$$

J: the total inertia given by:

$$J = \frac{J_{Turbine}}{G^2} + J_{generator}. \tag{11}$$

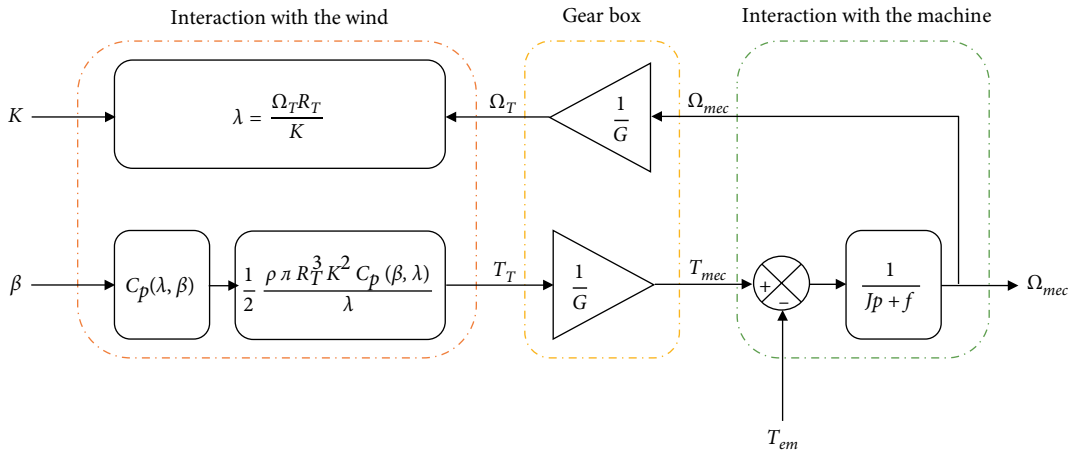

Figure 2: Block diagram of the turbine.

T_{vis}: the viscous friction torque.

$$T_{vis} = f\Omega_{mec}. \tag{12}$$

$$J\frac{d\Omega_{mec}}{dt} + f\Omega_{mec} = T_{mec} - T_{em} = \frac{C_T}{G} - T_{em}, \tag{13}$$

the block diagram of the turbine is given by Figure 2.

4. The DFIG Modelling Used in a WECS

The schematic representation of a DFIG in the three-phase reference is given in Figure 3.

The DFIG is represented in the park frame by the following equations:

The electrical equations are:

$$\begin{aligned} V_{sd} &= R_s I_{sd} + \frac{d\varphi_{sd}}{dt} - \omega_s \varphi_{sq}, \\ V_{sq} &= R_s I_{sq} + \frac{d\varphi_{sq}}{dt} + \omega_s \varphi_{sd}, \\ V_{rd} &= R_r I_{rd} + \frac{d\varphi_{rd}}{dt} - \omega_r \varphi_{rq}, \\ V_{rq} &= R_r I_{rq} + \frac{d\varphi_{rq}}{dt} + \omega_r \varphi_{rd}. \end{aligned} \tag{14}$$

The magnetic equations are:

$$\begin{aligned} \varphi_{sd} &= L_s I_{sd} + M I_{rd}, \\ \varphi_{sq} &= L_s I_{sq} + M I_{rq}, \\ \varphi_{rd} &= L_r I_{rd} + M I_{sd}, \\ \varphi_{rq} &= L_r I_{rq} + M I_{sq}. \end{aligned} \tag{15}$$

The active and reactive stator's powers are:

$$\begin{aligned} P_s &= V_{sd} I_{sd} + V_{sq} I_{sq}, \\ Q_s &= V_{sq} I_{sd} - V_{sd} I_{sq}. \end{aligned} \tag{16}$$

For vector control of DFIG connected to a reliable grid (balanced three-phase system), the Park reference linked to the rotating field is chosen. By adopting the hypothesis of a stator resistance R_s as negligible (given the power of the DFIG), and that the stator flux φ_s is constant (while V_s is constant) and oriented along the axis d [10].

$$\begin{aligned} \varphi_{sd} &= \varphi_s = cte, \\ \varphi_{sq} &= 0, \end{aligned} \tag{17}$$

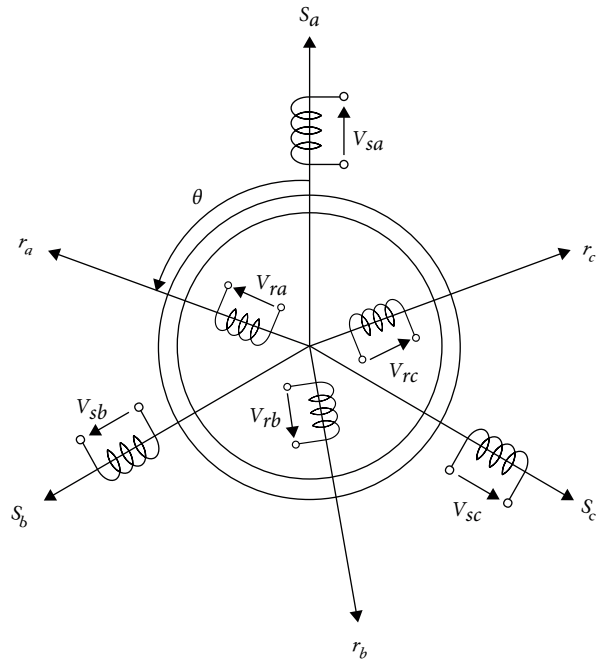

Figure 3: Representation of the DFIG in three-phase plan [9].

the following equations can be deduced from Equations: (14)–(16):

$$\begin{aligned} V_{sd} &= 0, \\ V_{sq} &= V_s = \omega_s \varphi_s, \\ V_{rd} &= R_r I_{rd} + \frac{d\varphi_{rd}}{dt} - \omega_r \varphi_{rq}, \\ V_{rq} &= R_r I_{rq} + \frac{d\varphi_{rq}}{dt} + \omega_r \varphi_{rd}, \end{aligned} \tag{18}$$

and

$$\begin{aligned} \varphi_{sd} &= \varphi_s = L_s I_{sd} + M I_{rd}, \\ 0 &= L_s I_{sq} + M I_{rq}, \\ \varphi_{rd} &= L_r I_{rd} + M I_{sd}, \\ \varphi_{rq} &= L_r I_{rq} + M I_{sq}. \end{aligned} \tag{19}$$

The stator currents are given by the following system:

$$I_{sd} = \frac{\varphi_s}{L_s} - \frac{M}{L_s} I_{rd},$$
$$I_{sq} = -\frac{M}{L_s} I_{rq}. \tag{20}$$

The active and reactive powers become:

$$P_s = V_{sq} I_{sq} = -\frac{M}{L_s} V_s I_{rq},$$
$$Q_s = V_{sq} I_{sd} = \frac{V_s \varphi_s}{L_s} - \frac{M V_s}{L_s} I_{rd}. \tag{21}$$

By injecting (20) in (19) the flux's equations are given by:

$$\varphi_{rd} = \left(L_r - \frac{M}{L_s}\right) I_{rd} + \frac{M \varphi_s}{L_s} = \left(L_r - \frac{M^2}{L_s}\right) I_{rd} + \frac{M V_s}{\omega_s L_s},$$
$$\varphi_{rq} = \left(L_r - \frac{M^2}{L_s}\right) I_{rq}. \tag{22}$$

By injecting (22) into (18) a new system of direct and quadrature rotor voltages is obtained:

$$V_{rd} = R_r I_{rd} + \left(L_r - \frac{M^2}{L_s}\right) \frac{dI_{rd}}{dt} - g\omega_s \left(L_r - \frac{M^2}{L_s}\right) I_{rq},$$
$$V_{rq} = R_r I_{rq} + \left(L_r - \frac{M^2}{L_s}\right) \frac{dI_{rq}}{dt} + g\omega_s \left(L_r - \frac{M^2}{L_s}\right) I_{rd} + g \frac{M V_s}{L_s}. \tag{23}$$

5. The Power Converters and Filter Modelling

5.1. The Power Converters Modelling. The simple voltages given at the output of the converter are [10]:

$$\begin{pmatrix} V_a \\ V_b \\ V_c \end{pmatrix} = \frac{E}{6} \begin{pmatrix} 2 & -1 & -1 \\ -1 & 2 & -1 \\ -1 & -1 & 2 \end{pmatrix} \begin{pmatrix} S_1 \\ S_2 \\ S_3 \end{pmatrix}. \tag{24}$$

5.2. The DC Link Modelling. It consists of a capacitor C placed between the two converters. It is governed by the following electrical equation:

$$\frac{dU_{dc}}{dt} = \frac{1}{C}\left(I_{GSC} - I_{RSC}\right). \tag{25}$$

I_{GSC}, I_{RSC}: are respectively the current at the converter output on the grid side and converter on the machine side.

5.3. The Filter Modelling. The filter is placed just after the source. It is composed of a resistor R in series with an inductance L called respectively the total resistance and inductance of the line.

The line voltages are given by:

$$V_{t1} = RI_{t1} + L\frac{dI_{t1}}{dt} + V_a,$$
$$V_{t2} = RI_{t2} + L\frac{dI_{t2}}{dt} + V_b,$$
$$V_{t3} = RI_{t3} + L\frac{dI_{t3}}{dt} + V_c. \tag{26}$$

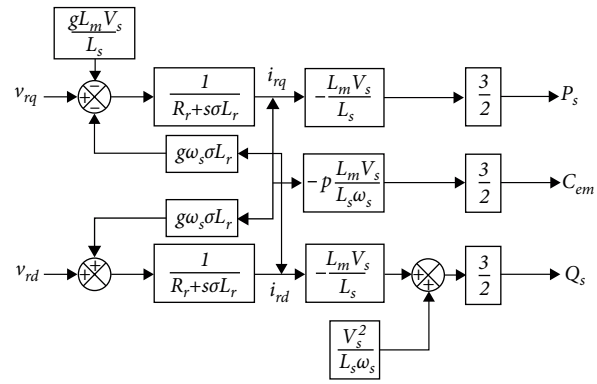

Figure 4: The DFIG's model [8].

6. The RSC's Control Using the PI Regulator

It exists 2 methods exist using the PI regulator:

(i) *Direct control:* This technique consists of directly and independently regulating the active and reactive stator powers produced to those of references, using a single regulator on each axis. The control is given by correcting the difference between the measured and the reference power, the regulator used is a PI controller.

(ii) *Indirect control without power loop:* This control does not consist in directly regulating the powers as the previous control but is based on the indirect regulation of the measured rotor currents which are controlled with the reference currents which are expressed as a function of the stator powers of reference imposed on the machine.

(iii) *Indirect vector control with power loop:* This command consists in regulating the stator powers and the rotor currents in cascade, for this we will set up two control loops on each axis with an integral proportional regulator for each, one regulating the power and the other the current.

In this paper the last one was chosen and its principal scheme is illustrated by Figure 4.

7. The RSC's Control Using the Sliding Mode

7.1. The Principle of the Sliding Mode. The sliding mode (SM) technique is developed from the variable structure control in order to solve the disadvantages of the other nonlinear control system designs namely the PI controller. Sliding mode is a technique that consists of initially defining a surface, the system that is controlled will be forced to that surface, and the system behavior is said to slide to the desired balance point. [7, 11–13].

The SM technique is mainly carried out in three complementary steps defined by:

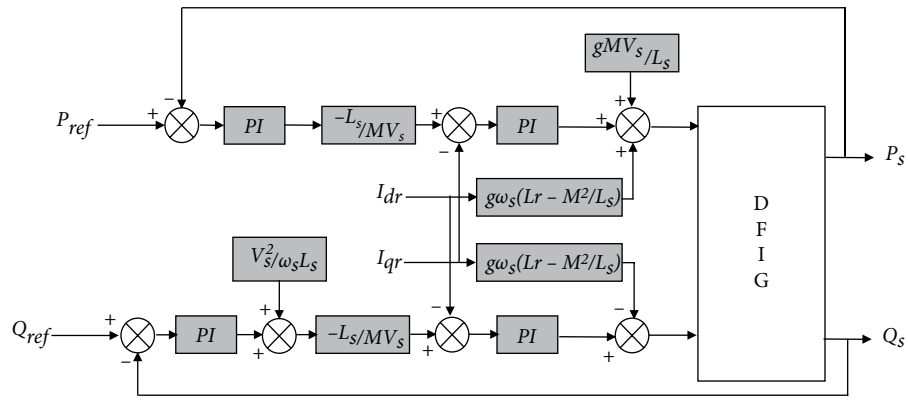

Figure 5: Indirect control of active and reactive power without power loop.

(i) The choice of sliding surface also called the switching surface.

(ii) The definition of conditions of existence and convergence of the control.

(iii) The determination of the control vector.

The main feature of this control as mentioned before is to drive the error to a "switching surface" $s(x)$. When the system is in "sliding mode", the system behavior is not affected by any modeling uncertainties and/or disturbances [14].

7.2. The Switching Surface Choice. The sliding surface $s(x)$ can be chosen in general as a hyperplane passing through the origin of space for stabilization reasons, the sliding surface that is a scalar function should be chosen such that the variable to be adjusted slides on this surface.

So its expression is as follows:

$$S(x) = \left(\frac{d}{dt} - \lambda\right)^{r-1} e(x). \tag{27}$$

(i) λ is positive gain that will interpret the bandwidth of the desired control.

(ii) $e(x)$ is the variable's error to be regulated.

(iii) r is the relative degree; it is the smallest positive integer representing the number of times to derive in order to display the command.

7.3. The Control's Conditions for Existence. The conditions of existence and convergence are the points that allow the different dynamics of the system to converge towards the sliding surface and to remain there independent of the perturbation.

It exists 2 approaches:

The direct approach: it consists on:

$$s(x) \cdot \dot{s}(x) < 0. \tag{28}$$

The Lyapunov's approach, it consists of choosing a Lyapunov's candidate function $v(x) > 0$ (scalar positive function) and a vector control that will decrease its derivative.

$$\dot{v}(x) < 0. \tag{29}$$

Basicall the Lyapunov's candidate function is chosen as follow:

$$v(x) = \frac{1}{2} s(x)^2. \tag{30}$$

7.4. The Determination of the Control Vector. The control function will satisfy reaching conditions in the following form:

$$U = U_{eq} + U_{com}, \tag{31}$$

where:

(i) U_{eq} is the equivalent or nominal control is determined by the system model.

U_{com} the sliding control: it consists of the sign function *sign* of the sliding surface $S(x)$, multiplied by a constant k_x.

$$U_{com} = k_x \cdot signs(x). \tag{32}$$

7.5. The RSC's Control Vectors Using the SM Technique. The purpose of this paragraph was to synthesize a control law based on the SM technique applied to the rotor-side converter to control the active and reactive powers generated by the DFIG's stator at the desired values.

The model used for the DFIG is the oriented stator flux model presented above (Figure 5), the electrical quantities of which are all expressed in a fixed reference frame linked to the stator. (d, q). Equations (18)–(21).

From Equation (21), controlling the power is controlling the rotor currents so the rotor currents are given by:

$$\begin{aligned} I_{rq} &= -\frac{L_s}{MV_s} P, \\ I_{rd} &= -\frac{L_s}{MV_s} Q + \frac{V_s}{\omega_s M}. \end{aligned} \tag{33}$$

The rotor currents' references are given by:

$$\begin{aligned} I_{rq}^{ref} &= -\frac{L_s}{MV_s} P^{ref}, \\ I_{rd}^{ref} &= -\frac{L_s}{MV_s} Q^{ref} + \frac{V_s}{\omega_s M}. \end{aligned} \tag{34}$$

(i) The switching surface choice

The active and reactive powers are proportional to the rotor currents, so can take r=1.

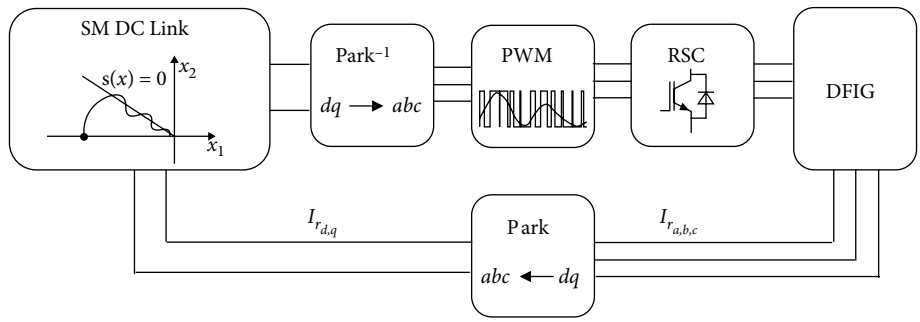

Figure 6: Control scheme of the RSC using the SM controller.

The switching surface's expression is as follows:

$$s(P) = I_{rq}^{ref} - I_{rq}, \tag{35}$$

$$s(Q) = I_{rd}^{ref} - I_{rd}. \tag{36}$$

(ii) The conditions of existence

The main objective is that the rotor currents follow their reference, so we can impose that:

$$s(P) = s(Q) = 0. \tag{37}$$

The SM will exist only if the following condition is met:

$$s(P).\dot{s}(P) \leq 0. \tag{38}$$

and

$$s(Q).\dot{s}(Q) \leq 0. \tag{39}$$

(iii) The control vector

From Equation (32) we have:

$$\begin{aligned} V_{rq} &= V_{rq_{eq}} + V_{rq_{com}}, \\ V_{rd} &= V_{rd_{eq}} + V_{rd_{com}}, \end{aligned} \tag{40}$$

where:

$V_{r_{eq}}$ is the equivalent command; $V_{r_{com}}$ is the sliding's command.

(iv) Calculation of the control vector

$$\dot{s}(P) = \dot{I}_{rq}^{ref} - \dot{I}_{rq}, \tag{41}$$

$$\dot{s}(Q) = \dot{I}_{rd}^{ref} - \dot{I}_{rd}. \tag{42}$$

By replacing the currents derivatives by their expressions (Equations (27) and (34)) we have:

$$\dot{s}(P) = \left(-\frac{L_s}{MV_s}\dot{P}^{ref} - \frac{1}{\sigma L_r}\left(V_{rq} - R_r I_{rq} - g w_s \sigma L_r I_{rd} - g\frac{MV_s}{L_s}\right)\right), \tag{43}$$

$$\dot{s}(P) = -v_1 sing(s(P)), \tag{44}$$

$$V_{rq} = -\frac{L_s \sigma L_r}{MV_s}\dot{P}^{ref} + R_r I_{rq} + g w_s L_r \sigma I_{rd} + g\frac{MV_s}{L_s} + L_r \sigma v_1 sgn(s(P)), \tag{45}$$

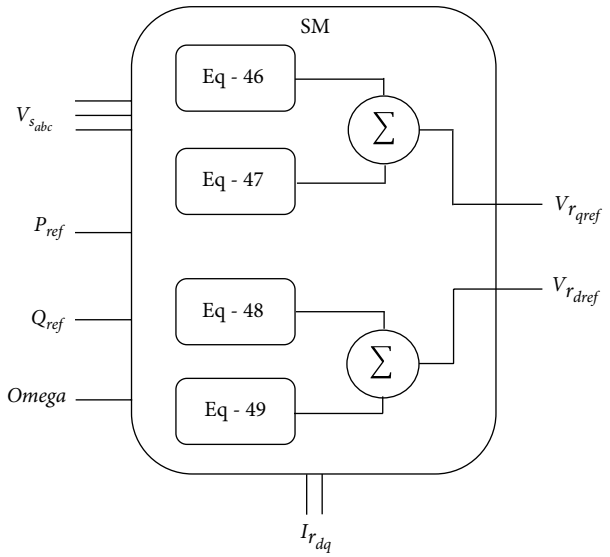

Figure 7: The SM's model.

$$V_{rq_{eq}} = -\frac{L_s \sigma L_r}{MV_s}\dot{P}^{ref} + R_r I_{rq} + g w_s L_r \sigma I_{rd} + g\frac{MV_s}{L_s}, \tag{46}$$

$$V_{rq_{com}} = L_r \sigma v_1 sgn((s(P))). \tag{47}$$

We have to redo the same calculation to find the control vector of the reactive power.

$$V_{rd_{eq}} = L_r \sigma\left(-\frac{L_s}{MV_s}\dot{Q}^{ref} + \frac{V_s}{Mw_s}\right) + R_r I_{rd} - g w_s L_r \sigma I_{rq}, \tag{48}$$

$$V_{rd_{com}} = L_r \sigma v_2 sgn((s(Q)). \tag{49}$$

After all this calculation the RSC controller's principle scheme using the SM is illustrated by Figure 6, and more detailed in Figure 7.

8. The GSC's Control

The purpose of the grid side converter's control was to control two large quantities therefore the control can be divided into two parts:

(i) Check the DC bus voltage and set it to a reference value.

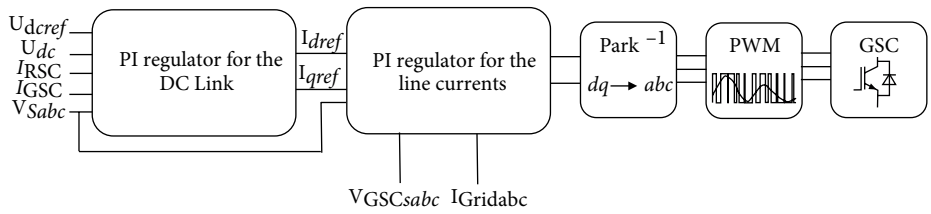

Figure 8: Control scheme of the GSC using the PI regulators.

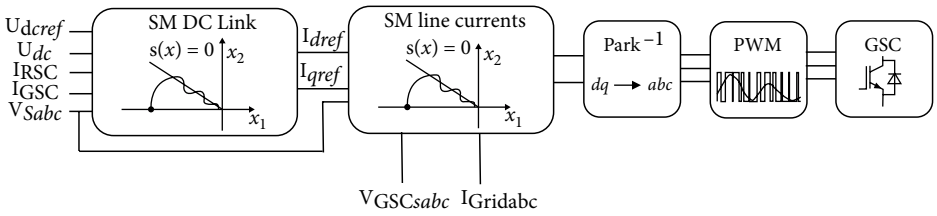

Figure 9: Control scheme of the GSC using the SM controller.

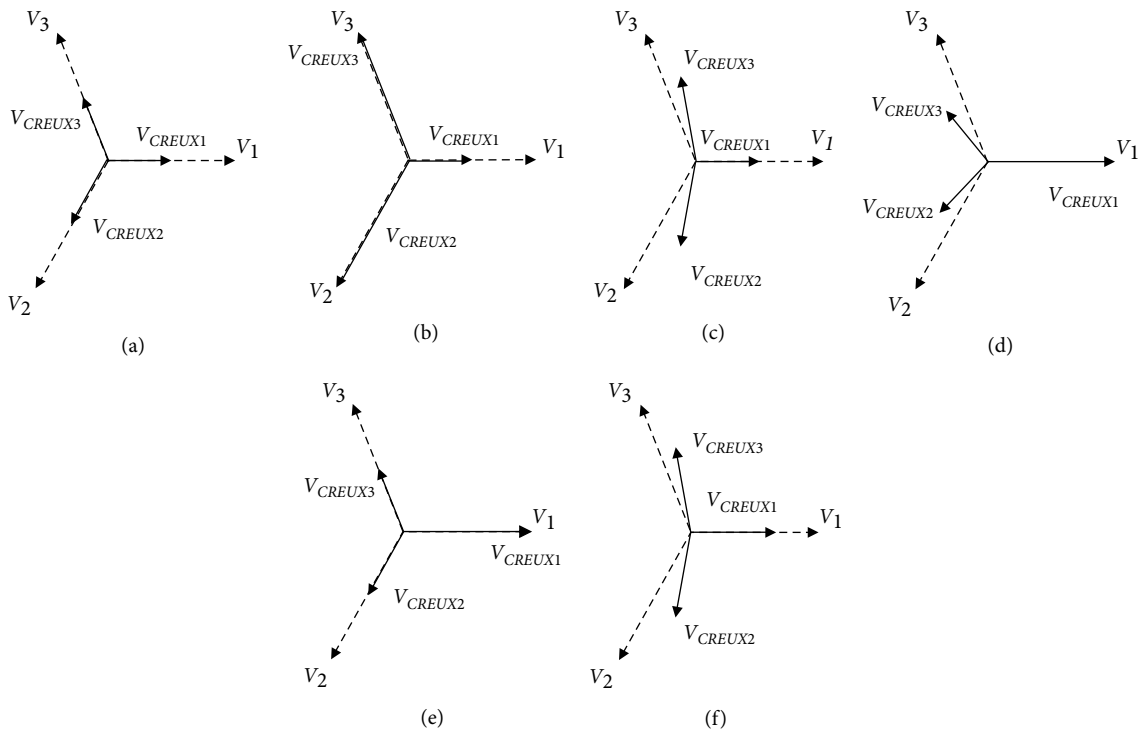

Figure 10: Classification of voltage dips [6].

(ii) Control reference reactive power to zero to ensure a unit power factor.

In fact, controlling the GSC is like controlling the active power by keeping the DC link voltage constant, and setting the reference reactive power to zero so as not to impair the quality of the grid (unit grid power factor).

8.1. The GSC's Control Using PI Regulators. This method is little used because of the disadvantages it brings, its principle is illustrated in Figure 8. It consists of synthesizing PI regulators.

8.2. The GSC's Control Using the SM Technique. This technique consists of developing a control law based on the sliding mode, so just follow the steps explained previously. The principle scheme is illustrated in Figure 9.

To elaborate the control laws of the two SMDC Link and SM Line current blocks, Equations (25) and (26) are used, and the same steps already explained before are followed.

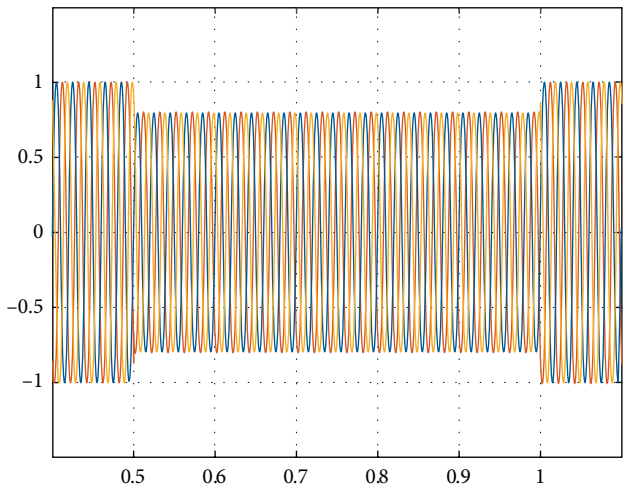

Figure 11: Stator voltages.

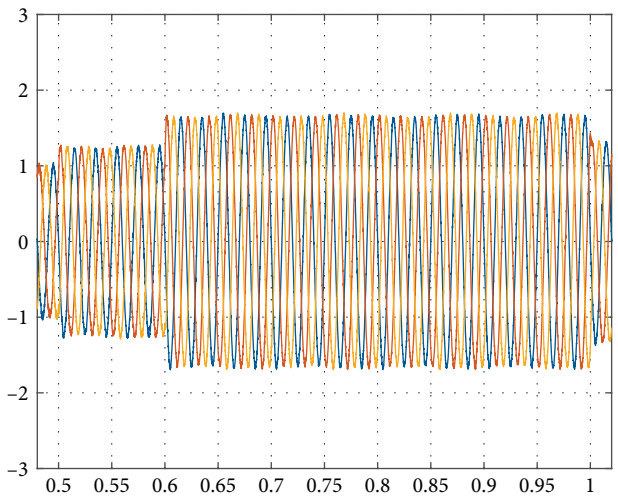

Figure 12: Stator currents.

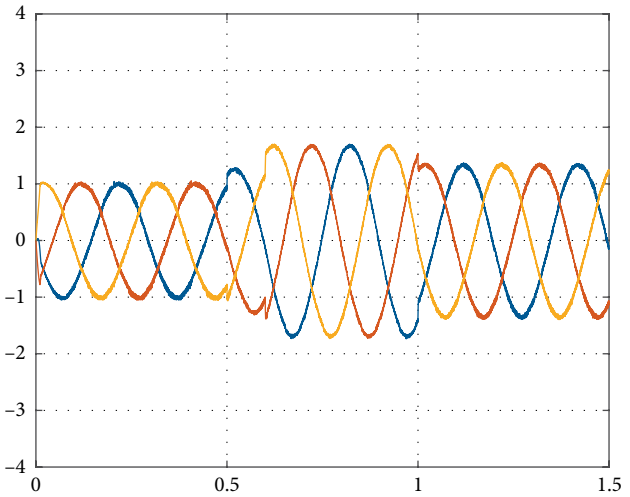

(a)

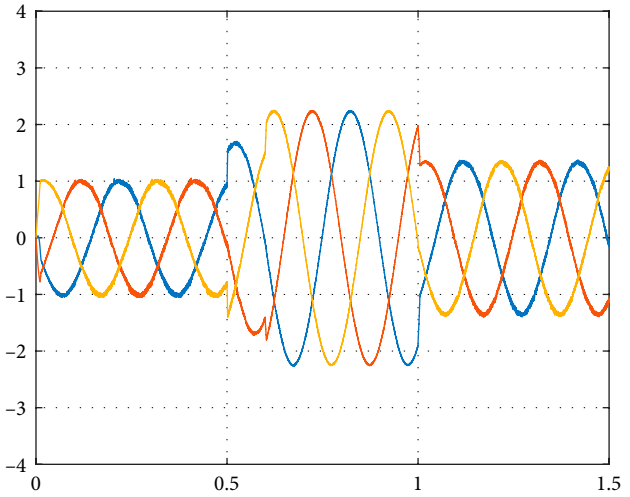

(b)

Figure 13: Rotor currents.

9. The Voltage Dips

A grid fault is physically, a short circuit occurring somewhere in the network, a voltage dip (voltage dips) being the repercussion of this fault on the voltage. A voltage dip is a sudden decrease in the supply voltage U to a value below a threshold value, followed by its recovery after a short time [6].

There are different types of voltage dips as shown in the Figure 10:

The stator voltage drop resulting from voltage dips gives rise to the following insurmountable effects:

(i) Increase in stator and rotor currents.

(ii) Decrease in the DC bus voltage or even destabilization.

(iii) Disturbance in the produced power.

Increasing currents can cause the over-size of the rotor side converter to support this extra current while the decrease of the voltage of the continuous bus can cause a disconnection of the wind turbine.

10. The Simulation Results

The simulation was carried out with MATLAB/Simulink, in order to validate the control strategies studied in this work. Simulation tests are realized with a 300 KW generator coupled to a 398 V/50 Hz grid and for a fixed wind speed because it is assumed that the duration of the fault is so short that the speed remains constant. The machine's parameters are given next in the Tables 1 and 2.

The different quantities are expressed in reduced unit (P.U), as an example the power in reduced unit is expressed as follows:

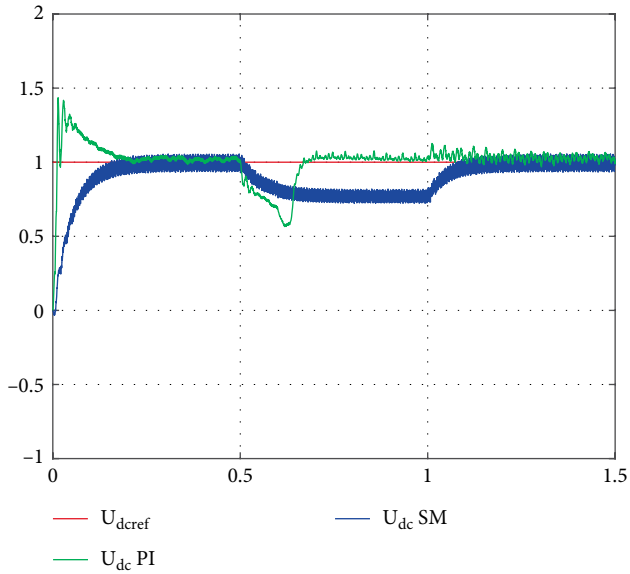

Figure 14: DC BUS voltage with 20% depth of stator voltage.

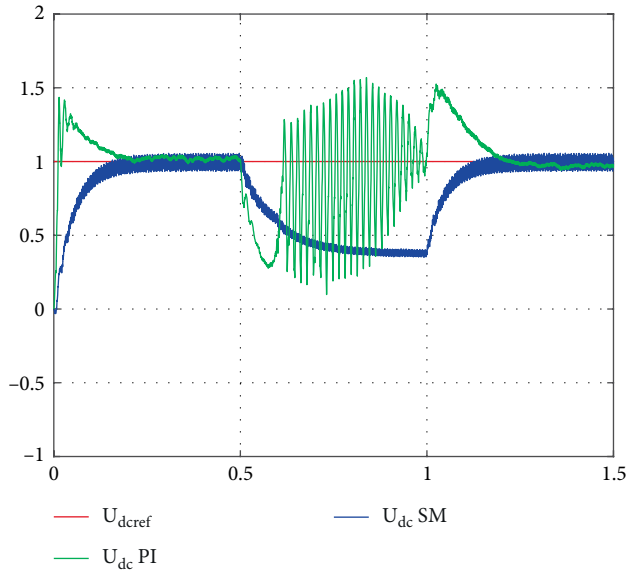

Figure 15: DC BUS voltage with 40% depth of stator voltage.

$$P_{pu} = \frac{P}{P_{nom}}. \tag{50}$$

The voltage dip is applied from $t = 500$ ms and lasts up to $t = 1000$ ms, for different depths: 20% and 40%.

Figure 11 shows the stator voltages with the voltage dip at $t = 500$ ms.

Figure 12 represents the stator currents that increase at the onset of the fault (explained in part 8).

Figure 13 shows the rotor currents for different depths: 20% for Figure 13(a) and 40% for Figure 13(b). It can be clearly noticed that the deeper the fault is, the higher the current increases.

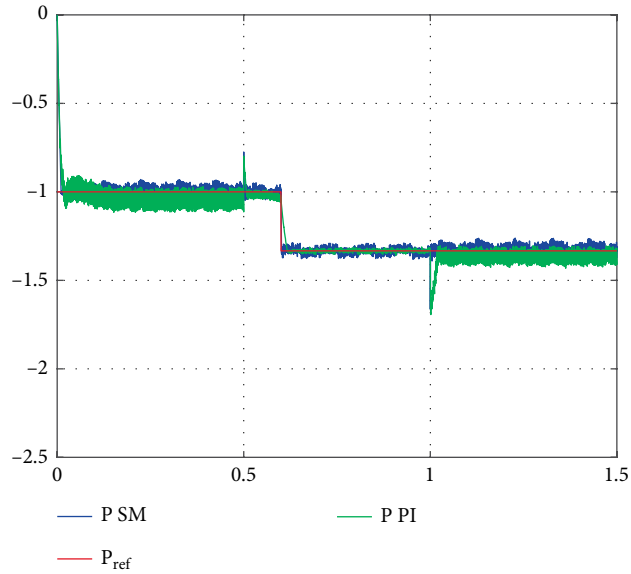

Figure 16: Active power with 20% depth of stator voltage.

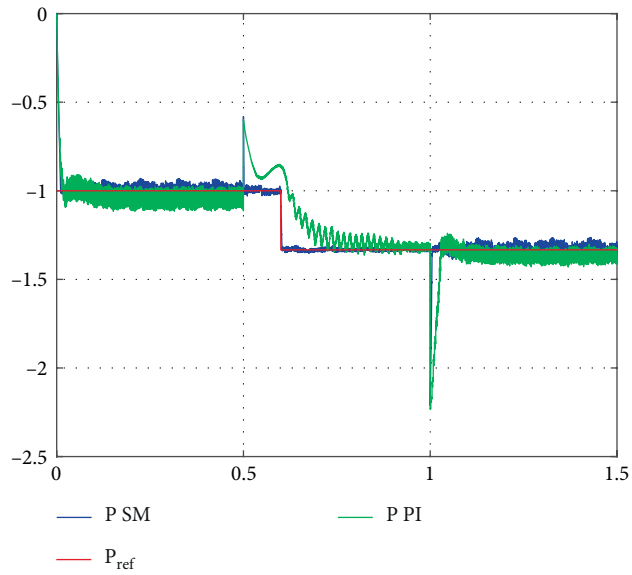

Figure 17: Active power with 40% depth of stator voltage.

Figures 14 and 15 successively give the shape of the DC bus in the presence of voltage dips for control of the GSC using PI regulators, and the sliding mode technique.

It can be observed that before the arrival of the default the voltage exactly follows its instruction for both types of commands, once the default has arrived the bus voltage is disturbed in both cases, except that for the command with PI, the voltage gives strong oscillations for a very deep default, that last as long as default is present. While for the control with SM the voltage is shifted from that of reference—this shift, is even larger than the depth of the default, is important.

Table 1: Doubly fed induction generator parameters.

Parameter	Symbol	Value
Rated power	P_n	300 kW
Frequency	f	50 Hz
Stator resistor	R_s	8.9 mΩ
Rotor resistor	R_r	13.7 mΩ
Stator inductor	L_s	12.9 mH
Stator inductor	L_r	12.7 mH
Mutual inductor	$L_m; M$	12.672 mH
Dispersion coefficient	σ	0.0198
Number of pole pairs	P	2

Table 2: Filter and grid parameters.

Parameter	Symbol	Value
Inductor	L	0.005 H
Resistor	R	0.25 Ω
Capacitor	C	4400 μF

Figures 16 and 17 show the active power developed by the DFIG. It is assumed that the power set point changes at time $t = 600$ ms and the remainder until the end of the simulation, it can be seen that for the control with PI the power is disturbed at the moment of the application of the hollow at significant depth, and the remainder until the disappearance of the latter, as for the command with SM with a very deep drop, we only notice spikes at the appearance and the disappearance of the drop, while the power perfectly follows his instructions.

A summary of the comparison results is presented in Tables 3 and 4.

Table 3: Comparison results for 20% depth of stator voltage.

	PI controller	SM
I_s	Increase	
I_r	Increase	
U_{DC}	Decreases by 40% for 500 ms then returns to its reference with oscillations	Stable decreases by 20%
P	Appearance of an overshoot then returns to its reference after a short response time	Appearance of an overtaking then immediately returns to its reference

Table 4: Comparison results for 40% depth of stator voltage.

	PI controller	SM
I_s	Increase	
I_r	Increase	
U_{DC}	Oscillates between 50% and −80%	Stable decreases by 60%
P	Appearance of an overshoot then returns to its reference after a short response time	Appearance of an overtaking then immediately returns to its reference

11. Conclusion

The purpose of this paper is to develop the control law using the sliding mode for both converters (GSC and RSC). The study is based on a comparison between a system whose GSC is based on a conventional PI controller and a second made by sliding mode taking into account the voltage dips to highlight the performance.

Finally, the simulation results showed that the control of the GSC using sliding mode, and during a voltage dip, is more efficient than the control using PI regulator.

Nomenclature

Ω_T: turbine speed
V_{sd}, V_{sq}: the dq axis stator voltages
I_{sd}, I_{sq}: the dq axis stator current
φ_{sd}, φ_{sq}: the stator d and q axis fluxes
V_{rd}, V_{rq}: the dq axis rotor voltages
I_{rd}, I_{rq}: the dq axis rotor current
φ_{rd}, φ_{rq}: the rotor d and q axis fluxes
R_s, R_r: stator and rotor resistances
ω_s, ω_r: the supply and rotor angular frequency
$V_{a,b,c}$: are the single voltages from the converter
$S_{1,2,3}$: are the MLI commands applied to the switches of the converter
E: is the DC voltage that comes from the DC link
$V_{t1,2,3}$: are the three-phase system of the source (the grid)
$V_{a,b,c}$: are the single voltages from the converter
$I_{t1,2,3}$: are the line currents coming from the source.

Data Availability

The data used to support the findings of this study are available from the corresponding author upon request.

Conflicts of Interest

The authors declare that they have no conflicts of interest.

References

[1] Hamane, B., M. L. Doumbia, M. Bouhamida, A. Draou, H. Chaoui, and M. Benghanem, "Comparative study of PI, RST, sliding mode and fuzzy supervisory controllers for DFIG based wind energy conversion system," *International Journal of Renewable Energy Resarch*, vol. 5, no. 4, pp. 1174–1185, 2015.

[2] M. El azzaoui, H. Mahmoudi, K. Boudaraia, and C. Ed-dahmani, "FPGA implementation of super twisting sliding mode control of the doubly fed induction generator," in *14th International*

Multi-Conference on Systems, Signals & Devices (SSD), IEEE, Marrakech, Morocco, 2017.

[3] N. El Ouanjli, M. Taoussi, A. Derouich, A. Chebabhi, A. El Ghzizal, and B. Boussoufi, "High performance direct torque control of doubly fed induction motor using fuzzy logic," *Gazi University Journal of Science*, vol. 31, no. 2, pp. 532–542, 2018.

[4] N. El Ouanjli, A. Derouich, A. El Gzizal, Y. El Mourabet, B. Bossoufi, and M. Taoussi, "Contribution to the performance improvement of doubly fed induction machine functioning in motor mode by the DTC control," *International Journal Power Electronics and Drive System*, vol. 8, no. 3, pp. 1117–1127, 2017.

[5] R. Chakib, "Commande avancée d 'une éolienne à base de la MADA en vue de sa participation aux services système : réglage de fréquence, réglage de tension et tenue aux creux de tension," 2017.

[6] S. ELAimani, "Modelisation de differentes technologies d'eoliennes integrees dans un reseau de moyenne tension," p. 217, 2004.

[7] H. Elaimani, A. Essadki, N. Elmouhi, and R. Chakib, "The modified sliding mode control of a doubly fed induction generator for wind energy conversion during a voltage dip," in *International Conference on Wireless Technologies, Embedded and Intelligent Systems (WITS)*, IEEE, Fez, Morocco, 2019.

[8] H. Elaimani and A. Essadki, "The study of the PI controler and the sliding mode of DFIG used in a WECS," in *International Renewable and Sustainable Energy Conference (IRSEC)*, IEEE, Tangier, Morocco, 2017.

[9] R. Chakib, A. Essadki, and M. Cherkaoui, "Active disturbance rejection control for wind system based on a DFIG," *International Journal of Electrical and Computer Engineering*, vol. 8, no. 8, pp. 1249–1258, 2014.

[10] T. Ghennam, *Supervision d'une ferme éolienne pour son intégration dans la gestion d'un réseau électrique, Apports des convertisseus multi niveaux au réglage des éoliennes à base de machine asynchrone double alimentation [Ph.D. thesis]*, HAL, Lyon, France, 2011.

[11] K. Belgacem, A. Mezouar, and A. Massoum, "Sliding mode control of a doubly-fed induction generator for wind energy conversion," *International Journal of Energy Engineering*, vol. 2013, no. 1, pp. 30–36, 2013.

[12] M. Smaili, "Par modélisation et commande d'un aérogénérateur à machine asynchrone à double alimentation en vue de simulation des problèmesde cogénération," 2013.

[13] B. Beltran, M. E. H. Benbouzid, T. Ahmed-Ali, "High-order sliding mode control of a dfig-based wind turbine for power maximization and grid fault tolerance," in *IEEE International Electric Machines and Drives Conference*, IEEE, pp. 183–189, Miami, FL, USA, 2009.

[14] R. Riyadh, "Contrôle des puissances générées par un système éolien à vitesse variable basé sur une machine asynchrone doublealimentée," 2016.

[15] Y. Djeriri, "Commande directe du couple et des puissances d 'une MADA associée à un système éolien par les techniques de l'intelligence artificielle," 2015.